

Itinerant ferromagnetism in repulsively interacting spin-orbit coupled Fermi gas

Shang-Shun Zhang^{1,2}, Jinwu Ye^{2,3}, and Wu-Ming Liu¹

¹*Beijing National Laboratory for Condensed Matter Physics,*

Institute of Physics, Chinese Academy of Sciences, Beijing 100190, China

²*Department of Physics and Astronomy, Mississippi State University, MS 39762, USA*

³*Key Laboratory of Terahertz Optoelectronics, Ministry of Education,
Department of Physics, Capital Normal University, Beijing 100048, China*

(Dated: December 6, 2024)

We investigate the itinerant ferromagnetism of repulsively interacting Fermi gases with spin-orbit coupling (SOC). We find that a strong SOC can considerably reduce the critical interaction strength for itinerant ferromagnetism (FM) transition, which provides a new and efficient mechanism to realize this long sought state. Near the FM transition, the coexistence of two types of spin fluctuations induced by SOC leads to new quantum-classical crossover regimes. In the FM side, the Fermi surfaces acquire a finite momentum and also experience a topological Lifshitz transition driven by the magnetization, the symmetry breaking leads to two gapped transverse pseudo-Goldstone modes instead of gapless Goldstone modes, both of which are dramatic SOC effects. These novel phenomena can be detected by the current experimental techniques in cold atoms.

PACS numbers: 03.75.Ss, 03.75.Kk, 67.10.Db

Introduction.— Nowadays, investigation of spin-orbit coupling (SOC) has become subject of intensive research in cold atoms. The recent experimental realizations of 1D SOC [1–4] and the proposals to realize the 2D Rashba and 3D isotropic SOC [5–7] for neutral cold atoms inspired extensive theoretical investigations on pairing physics of attractive Fermi gases with SOC [8–14], which display various important SOC effects due to its unique symmetry, single particle behavior and absence of Galileo invariance. However, there are still relatively few works in the repulsive side which could display quite different symmetry breaking orders than that in the attractive side [15–17], and the effects of SOC on these different symmetry breaking phases need to be addressed.

For itinerant fermions with strong short-range repulsion, there exists a ferromagnetic phase transition, i.e., the so-called Stoner’s instability [18–24]. This textbook model provides a qualitative understanding of the itinerant ferromagnetism (FM), which is a fundamental phenomena in nature, but not yet tested straightforwardly in experiment. Recent years, cold atom provides an ideal platform to study itinerant FM due to its cleanness and highly tunability. There were both experimental [25] and theoretical work [26–28] on possible FM in a purely repulsively interacting two component Fermi gas of ⁶Li atoms. However, the fast decay to molecular state due to the strong interaction strength of FM transition makes the itinerant FM actually unobservable [29–32].

In this Letter, we show that a repulsively interacting Fermi gas with 3D isotropic SOC provides an efficient way to fulfill this target. We find that the critical interaction strength for the itinerant FM state is greatly reduced due to the flat-band structure near the bottom of the spectrum, which would overcome the shortcoming due to the fast decay to molecular state. Besides this distinct advantage, the synthetic SOC leads to a list

of novel phenomena not shared by an ordinary Fermi gas without SOC. We construct a quantum Ginsburg-Landau effective action to describe critical magnetic fluctuations near the paramagnet to the FM transition [33–35], which obeys the unique symmetry breaking $[SU(2)_{spin} \times SO(3)_{orbit}]_D \rightarrow [U(1)_{spin}^z \times SO(2)_{orbit}]_D$ (the D stands for the simultaneous rotation of spin and orbit) due to SOC. The coexistence of the transverse and longitudinal spin modes with different dynamic exponents lead to new quantum-classical crossover regimes in the $T - r$ plane. In the FM side, there are three main new features which are dramatically different than those without SOC [36]: (I) The FM ground state acquires a non-zero momentum opposite to the direction of the magnetization, which can be detected by absorption-imaging the atom cloud after Time of Flight (TOF) [1]. (II) Increasing the magnetization will drive a topological Lifshitz phase transition, which has experimentally detectable critical behaviors in density of states, specific heat and compressibility [37–43]. (III) Due to the spin-momentum locking, the symmetry breaking here leads to two gapped transverse pseudo-Goldstone modes instead of the Goldstone modes. In view of the rapid technical developments of cold atoms in speckling, tomographic and *In-Situ* measurements [43–46], our theoretical predictions could be probed in near future experiments in both cold atoms and relevant condensed matter systems.

General formulation.— We consider a repulsively interacting two-component Fermi gas with the isotropic Weyl SOC, described by the Hamiltonian

$$\mathcal{H} = \sum_{\mathbf{k}, \alpha, \beta} \Psi_{\mathbf{k}, \alpha}^\dagger \left(\frac{\hbar^2 \mathbf{k}^2}{2m} + \lambda \mathbf{k} \cdot \boldsymbol{\sigma} - \mu \right)_{\alpha, \beta} \Psi_{\mathbf{k}, \beta} + g \sum_{\mathbf{k}, \mathbf{p}, \mathbf{q}} \Psi_{\mathbf{k}+\mathbf{q}, \uparrow}^\dagger \Psi_{\mathbf{p}-\mathbf{q}, \downarrow}^\dagger \Psi_{\mathbf{p}, \downarrow} \Psi_{\mathbf{k}, \uparrow}, \quad (1)$$

where $\lambda = \frac{g_F \mu_B \nabla B}{3m\hbar}$ is the SOC strength with ∇B the magnetic field gradient in the scheme [5, 6], g_F the Landé factor and μ_B the Bohr magneton, $g = \frac{4\pi a_s}{m}$ with a_s the positive s -wave scattering length. The chemical potential μ is determined by the atoms density self-consistently.

The interaction can be divided into the density and spin channel $\mathcal{H}_I = \frac{g}{8} \int d\mathbf{r} [\rho(\mathbf{r})^2 - \vec{S}(\mathbf{r})^2]$, where $\rho(\mathbf{r}) = \Psi^\dagger \Psi(\mathbf{r})$ and $\vec{S}(\mathbf{r}) = \Psi^\dagger \vec{\sigma} \Psi(\mathbf{r})$. In the presence of SOC, the density fluctuation is coupled with the spin fluctuation [16]. We introduce the density-spin order parameter ϕ_μ , $\mu = n, x, y, z$ to decouple the interaction term via a Hubbard-Stratonovich transformation. Integrating out the fermionic fields leads to the effective action for ϕ_μ :

$$S_H = \int d\mathbf{r} \int_0^{1/T} d\tau \frac{1}{2g} \phi_\mu^2 - \text{Tr} \ln (-\mathcal{G}_0^{-1} + M), \quad (2)$$

where $\mathcal{G}_0^{-1} = -\partial_\tau - \mathcal{H}_0 + \mu$, $M = \frac{i}{2} \phi_n \sigma^0 + \frac{1}{2} \vec{\phi} \cdot \vec{\sigma}$.

In the vicinity of the QCP, the magnetic order parameter $\vec{\phi}$ can be taken as a small quantity. However, the density channel ϕ_n has a non-zero *imaginary* saddle point value due to the finite particle density of the fermions which could be eliminated by re-defining ϕ_n as the deviation from its saddle point value. To the second order of ϕ_μ , we obtain $S_H^{(2)} = 1/(2\beta V) \sum_{\mathbf{q}, n} \mathcal{K}^{\mu\nu} \phi_\mu(-\mathbf{q}, -i\omega_n) \phi_\nu(\mathbf{q}, i\omega_n)$, where $\mathcal{K}^{\mu\nu} = \delta^{\mu\nu}/g - \bar{\chi}^{\mu\nu}(\mathbf{q}, i\omega_n)/4$, $\bar{\chi}^{\mu\nu}$ is related to the usual density-spin susceptibility $\chi^{\mu\nu}(\mathbf{q}, i\omega_n) = \langle s^\mu(\mathbf{q}, i\omega_n) s^\nu(-\mathbf{q}, -i\omega_n) \rangle$ via $\bar{\chi}^{00} = -\chi^{00}$, $\bar{\chi}^{0i} = i\chi^{0i}$, $\bar{\chi}^{ij} = \chi^{ij}$ with $i, j, = x, y, z$.

Collective modes in the paramagnetic phase.— Adding density-spin sources to Eq. (2), one can extract collective modes through the poles of density and spin correlation functions [16]. In the presence of SOC, it is convenient to introduce a helical basis with respect to the momentum where we can define two transverse spin modes ($\hat{T}_1 \cdot \vec{S}$, $\hat{T}_2 \cdot \vec{S}$) and one longitudinal spin mode ($\hat{q} \cdot \vec{S}$). In the paramagnet side, the mixing of density and longitudinal mode leads to one gapless sound mode $\omega_{\mathbf{q}}^s = v_s q$ and one gapped mode $\omega_{\mathbf{q}}^L = \Delta_s + \beta_L q^2$ called L mode in Fig.2a. There are also two degenerate gapped transverse modes $\omega_{\mathbf{q}}^{T_1} = \omega_{\mathbf{q}}^{T_2} = \Delta_s + \beta_T q^2$ just below the L mode (Fig.2a). We find Δ_s vanishes for interaction strength larger than $g_s = 24\pi^2 k_R / m(k_2^2 - k_1^2)$, where $k_2 > k_1$ are the two Fermi momenta. This corresponds to an instability in the collective modes channel. In the following section, we will show that the instability in the particle-hole (PH) channel happens first.

Ferromagnetic instability.— There is also a FM instability in the PH channel when $\delta = \frac{1}{g_c} - \frac{\chi_0}{4} < 0$, i.e., the Stoner instability. Here $\chi_0(\mathbf{q} \rightarrow 0, \omega = 0) = \frac{m}{6\pi^2} (\frac{k_1^2 + k_2^2}{K} + \frac{k_2^2 - k_1^2}{k_R})$, $K = \sqrt{k_R^2 + 2m\mu}$, $k_R = m\lambda$ is the static spin susceptibility of 3D free Fermi gas with the Weyl SOC. We obtain the critical value $k_F a_s^c = F(\gamma)$ as shown in Fig.1 (a), where k_F is the Fermi momentum

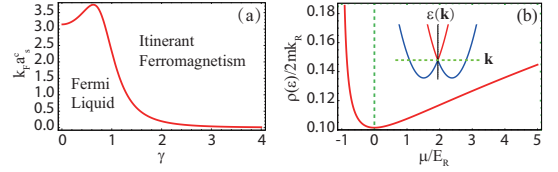


FIG. 1. (Color online) (a) Critical interaction strength $k_F a_s^c$ to the itinerant ferromagnetism as a function of SOC strength $\gamma = k_R/k_F$. (b) The density of states $\rho(\epsilon)$ in units of $2mk_R$ at the chemical potential μ . The green dashed line denotes $\mu = 0$ as shown by the inset.

without SOC at the same density and $\gamma = k_R/k_F$. As γ increases, $F(\gamma)$ has a maximum at $\gamma \simeq 0.63$ corresponding to the chemical potential $\mu = -\frac{2}{3} E_R$ ($E_R = k_R^2/2m$), after which, $k_F a_s^c$ decreases quickly. At a strong SOC, the μ approaches the bottom of the spectrum (the Weyl shell at $|\mathbf{k}| = k_R$) where the density of states diverges as $\frac{1}{\sqrt{\epsilon}}$ (see Fig.1 (b)). The effects of an interaction is dramatically enhanced, even a weak interaction will drive the system into the itinerant FM state.

Because $g_c < g_s$, so the instability in the PH channel happens before that in the collective mode channel. So in constructing a quantum Ginzburg-Landau action to describe the paramagnet-FM transition, one need to take the $\mathbf{q} \rightarrow 0, \omega/v_F q \rightarrow 0$ limit to capture the dominant critical spin-fluctuation spectral weights.

Ginzburg-Landau effective action in spin-orbit coupled systems.— Because the density fluctuation is non-critical across the FM phase transition, integrating it out and taking the $\mathbf{q} \rightarrow 0, \omega/v_F q \rightarrow 0$ limit leads to the effective action in terms of the spin fluctuation order parameter:

$$S_H = \int \frac{d\mathbf{k}}{(2\pi)^3} T \sum_n \frac{1}{2} \mathcal{G}_s^{-1} \hat{P}_s^{ij} \phi_i \phi_j + u \int d\mathbf{r} d\tau (\vec{\phi}^2)^2, \quad (3)$$

where $\hat{P}_s^{ij} = \hat{n}_s^i \hat{n}_s^j$ ($\hat{n}_s = \hat{T}_1, \hat{T}_2, \hat{L}$) is the projection operator into the helical basis, $\mathcal{G}_{T_1}^{-1} = \mathcal{G}_{T_2}^{-1} = \delta + \gamma_T y + \alpha_T q^2$ and $\mathcal{G}_L^{-1} = \delta + \gamma_L y^2 + \alpha_L q^2$ where $y = |\omega_n|/v_F q$ are the propagators of the helical spin modes. Note that the most relevant interaction term is still $S_H^{int} = u \int d\mathbf{r} d\tau (\vec{\phi}^2)^2$ which is $SU(2)_{spin} \times O(3)_{orbit}$ invariant. There are other quartic terms which contain momenta and only have $[SU(2)_{spin} \times O(3)_{orbit}]_D$ symmetry, so are less relevant. The effective action takes the same form for $\mu > 0$ or $\mu < 0$. Note that the transverse propagator with the dynamical exponent $z_T = 3$ is the same as the FM transition in the ordinary Fermi gas without SOC. While, the longitudinal one with a dynamical exponent $z_L = 2$ is similar to the anti-FM transition in the ordinary Fermi gas or dilute Bose gas transition without SOC.

Quantum-classical crossovers at finite temperatures.— Under the scaling transformation $q \rightarrow q'/b$, $\omega \rightarrow \omega'/b^z$, $z = 3$, at the tree level $\delta' = \delta b^2$, $\gamma'_L = \gamma_L b^{-2}$ and

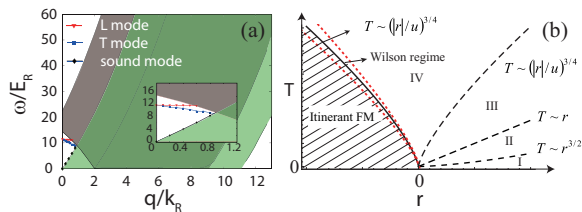


FIG. 2. (Color online) (a) Collective modes and particle-hole excitation in the paramagnet side at $\gamma = 0.2$, $a_s = 0.9a_s^c$. Inset is an enlarged drawing of the collective modes. (b) Finite temperature-classical crossovers near the para-magnet to FM transition. r is the tuning parameter of the transition and T is the temperature. The boundary line $T \sim r^{3/2}$ ($T \sim r$) indicates the quantum to classical crossover of the two transverse modes (one longitudinal mode). The line between Regime III and IV and also the Curie temperature are given by $T \sim (|r|/u)^{3/4}$ due to the dangerously irrelevant coupling u . The correlation length ξ and specific heat C_V display different behaviors in the four regimes as listed in the text.

$u' = ub^{4-d-z}$. Because $4 - (d+z) < 0$ in 3D, so u is dangerously irrelevant which leads to the violations of scalings holding only below the upper critical dimension[47]. Incorporating the RG flow of the irrelevant γ_L will recover the scaling of the longitudinal mode with the dynamical exponent $z_L = 2$. Following the combination of the RG methods developed in [35] and [48–50], we derived the whole crossover functions in the $T - r$ plane in Fig.2b for both the correlation length and the free energy. In the following, we only list the qualitative features.

We construct the RG flow equations at one-loop level and solve renormalized parameters [51] to the scale b_* with $\delta(b_*) = 1$, where mean field theory apply. If the renormalized temperature $Tb_*^{z_T}, Tb_*^{z_L} \ll 1$, the system stays in the quantum regime as shown by the regime I in Fig. 2. we obtain $\delta(b) = b^2(r + u\mathcal{A}_T T^2/r)$ with $r = \delta - \delta_c$. The correlation length $\xi^{-1/\nu} = r + u\mathcal{A}_T T^2/r$ with $\nu = 1/2$ displays the Fermi liquid behavior. Self-consistency requires $T < r^{z_T\nu} = r^{3/2}$ for this regime I. The contribution from the longitudinal mode remains exponentially small.

In regime II, $r^{3/2} < T < r$, the transverse modes become classical while the longitudinal mode remains quantum-like. The correlation length is given by $\xi^{-2} = r + 2u\mathcal{C}_T T^{4/3}$ where $\mathcal{C}_T = \mathcal{A}_T + \mathcal{B}_T$ [51]. The contribution from the longitudinal mode remains exponentially small.

In regime III and IV, $T \gg r$, both the transverse and the longitudinal mode behaves classically. The correlation length is given by $\xi^{-2} = r + 2u\mathcal{C}_T T^{4/3} + u\mathcal{C}_L T^{3/2}$ where the contribution from the longitudinal mode is subleading to that from the transverse mode due to $z_L < z_T$. Comparing the relative importance of r and $2u\mathcal{C}_T T^{4/3}$ leads to $T \sim (r/2u\mathcal{C}_T)^{3/4}$ separating the two sub-regimes III and IV shown in Fig.2b. Setting $\xi^{-2} = 0$ leads to the finite Curie temperature $T_c(r, u) =$

$(-r/2u\mathcal{C}_T)^{3/4}$. Within a narrow window close to $T_c(r, u)$ (between the red dotted lines in Fig. 2 (b)), the system is controlled by the classical Wilson-Fisher fixed point.

The free energy density is the sum of that from the two transverse modes $2\mathcal{F}_T$ and that from the longitudinal mode \mathcal{F}_L . The \mathcal{F}_T is the same as that in the traditional Fermi liquid [35]. In addition to its regular part, the \mathcal{F}_L is given by a universal function $F_L(r, T) = T^{5/2}\Phi_L(\frac{r}{T})$ [52]. In the quantum regime of longitudinal mode I/II, $T/r \ll 1$, the specific-heat coefficient $\gamma_L = \frac{C_V}{T} = \frac{A_1}{r^{3/2}}T^2$ where $A_1 \simeq 1.316$. While in classical regime III/IV, $T/r \gg 1$, $\gamma_L = A_2 T^{1/2}$ where $A_2 \simeq 0.113$. We note that the longitudinal mode displays anti-FM like behaviors.

Properties in the itinerant FM side.— For $g > g_c$ ($\delta_s < 0$), it moves to the ferromagnetic side, the magnetization $\langle \vec{\phi} \rangle = -\frac{g}{2}\langle \vec{M} \rangle \neq 0$ can pick up any direction (such as z direction) by moving the center of spin polarization away from the origin (Figs. 3 (d)-(f)), which breaks the $[SU(2)_{spin} \times O(3)_{orbit}]_D$ symmetry to $[U^z(1)_{spin} \times U^z(1)_{orbit}]_D$. We find $M \sim (g - g_c)^{1/2}$ from the self-consistent equation which has the same critical exponent as the traditional case. Then we can re-define $\phi_{T1}, \phi_{T2}, \phi_L$ with respect to this direction (*Note that they are defined with respect to the momentum \mathbf{q} in the para-magnet side*). The fermionic spectrum as shown in Fig. 3 (a)-(c) is given by

$$\xi_{\mathbf{k},s} = k_{\perp}^2 + k_z^2 + 2s\sqrt{k_{\perp}^2 + (k_z - \zeta)^2}, \quad (4)$$

where $s = \pm, k_{\perp} = \sqrt{k_x^2 + k_y^2}$. We have taken the momentum unit $k_R = m\lambda$ and energy unit $E_R = k_R^2/2m$. The dimensionless value $\zeta = \frac{Mg}{4\lambda k_R}$ which denotes the strength of magnetization is the crossing point of the two helicity branches. The spectrum in Fig. 3 has a global minimum at $\mathbf{k} = -1\hat{e}_z$, independent of the value of ζ . The magnetization \vec{M} induces a FS shift along the $-\hat{e}_z$, which can be detected by absorption-imaging the atom cloud after TOF [1]. As expected, the local current density vanishes due to the presence of the SOC. For an given particle density with increasing ζ , we divide the FM phase into three regimes shown in the Fig.3.

In the weak FM near to the QCP: $\zeta \ll 1$ (Figs.3a,3d), there are still two FS. There are still one gapless sound mode and three gapped modes (see Fig.2a). Due to the symmetry breaking in the FM side, the effects of the small magnetization in Fig.2a are (1) the sound wave velocity becomes anisotropic $\omega = v(\theta)q$. (2) One gap in paramagnet side splits into two: $\Delta_L > \Delta_T$ and the dispersion near $\mathbf{q} = 0$ is linear along q_z direction. All the collective modes are still outside the PH spectrum, therefore remain stable. It is important to stress that this gapless sound mode is not a Goldstone mode. Because the spin-momentum locking, the symmetry breaking as mentioned above only leads to gapped pseudo-Goldstone modes instead of gapless Goldstone modes, in sharp con-

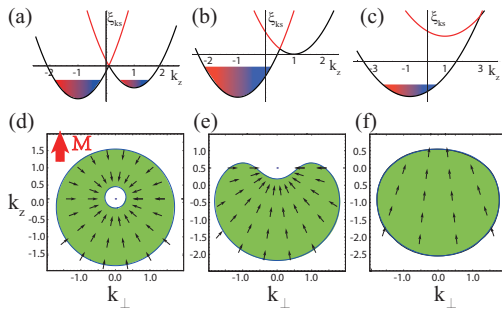


FIG. 3. (Color online) The topological Lifshitz phase transition tuned by the magnetization ζ where two fermi surfaces change into one near $\zeta \sim 0.3$. The fermionic spectrum $\xi_{\mathbf{k}_s}$ (upper panel) and Fermi surfaces (down panel) at the SOC strength $\gamma = 0.74$ at $\zeta = 0.1$ for (a),(d), $\zeta = 0.5$ for (b),(e), $\zeta = 3$ for (c),(f). The spectrum has a rotational symmetry about k_z axes. The black arrows show the spin polarization.

trast to the $SU(2)_{spin} \rightarrow U^z(1)_{spin}$ symmetry breaking in conventional Fermi systems without SOC.

As \vec{M} increases, there is a zero temperature topological Lifshitz transition [37] where the two FS changes into one FS near $\zeta \sim 1$ (Figs.3b,3e). Scaling functions near the Lifshitz transition in the density of states, specific heat and compressibility can be derived along the lines presented in [37]. The spin polarization changes as shown by the arrows. Due to the complicated FS geometry in Fig 5e, one can only perform numerical calculations. We find that the sound/L mode will start to fall into the intra-/inter- band PH continuum, therefore over-damped, then only the two transverse pseudo-Goldstone modes survive the Lifshitz transition.

In the strong FM: $\zeta \gg 1$ (Figs.3c,3f), there is a large energy separation between the two helicities. In the limit $\zeta \rightarrow \infty$, the fermionic spectrum reduces to $\xi_{\mathbf{k},s} = (\mathbf{k} - s\hat{e}_z)^2 - 2s\zeta - 1$, $s = \pm 1$. The spin approaches being polarized along the \hat{e}_z axis (Fig.5f). One can perform analytical calculations in such a simplified FS geometry and find that the two pseudo-Goldstone modes have an energy gap $\Delta_T \sim 4E_R$ at $\mathbf{q} = 0$, and behave as $\omega_{\mathbf{q}} = (\mathbf{q} - 2\hat{e}_z)^2/5$ near the roton minimum at $\mathbf{q} = 2\hat{e}_z$. At large, but finite ζ , the dispersion obtains a small imaginary part inside the intraband PH excitation shown in Fig. 4. The roton mode acquires a tiny gap [36].

Experimental implementation.— It was proposed that an arbitrary type of SOC could be constructed using a sequence of pulsed inhomogeneous magnetic fields imprinting suitable phase gradients on the atoms [5, 6]. In a ${}^6\text{Li}$ system, the two hyperfine sublevels $|1/2, -1/2\rangle$ and $|1/2, 1/2\rangle$ can be chosen as two pseudo-spin 1/2 states. With $N \sim 10^4$ ${}^6\text{Li}$ atoms inside an isotropic trap with a trap frequency $2\pi \times 10\text{Hz}$, and a typical magnetic field gradient strength $\nabla B = 0.09\text{G}/\mu\text{m}$ (within practical range [53]), we estimate the critical interaction strength

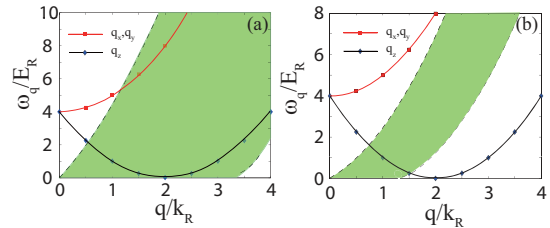


FIG. 4. (Color online) The collective modes and intra-band (“-” helicity) particle-hole excitation spectrum along q_z direction (green regimes) near the saturation limit $\zeta \gg 1$. (a) dense density case and (b) dilute density case. Due to its very high energy, inter-band one is outside the plotrange [36].

as $k_F a_s^c \simeq 0.19$, which is order of magnitude smaller than the value $\simeq 3\pi/4$ without the SOC [26–28, 33]. Monitoring spin fluctuations using speckle imaging [44, 45] or measuring the ground state momentum by absorption-imaging the atom cloud after TOF [1] could provide evidences of formation of magnetic domains. From a high resolution density image of atoms in a trap at finite temperature, one can also extract information about their critical behaviors near both the paramagnet to FM transition and the topological Lifshitz transition [38–43, 46].

In summary, we find that a strong SOC greatly reduces the critical interaction strength of FM transition in repulsively interacting Fermi system, which creates a rare favorable condition to realize this long sought state, whose realization in experiment would play a crucial role in the understanding of itinerant FM. The study here reveals dramatic SOC effects across the FM phase transition not shared by an ordinary Fermi system without SOC. The itinerant FM also displays the anomalous Hall effect and will be investigated in a future publication. This work can be easily extended to other cases with different SOC forms.

This work was supported by the NKBRSCF under grants Nos. 2011CB921502, 2012CB821305, NSFC under grants Nos. 61227902, 61378017, SPRPCAS under grants No. XDB01020300. J. Ye was supported by NSF-DMR-1161497, NSFC-11174210, Beijing Municipal Commission of Education under Grant No. PHR201107121.

-
- [1] Y. J. Lin, K. Jiménez-García, and I. B. Spielman, Nature (London) **471**, 83 (2011).
 - [2] P. Wang, Z. Q. Yu, Z. Fu, J. Miao, L. Huang, S. Chai, H. Zhai, and J. Zhang, Phys. Rev. Lett. **109**, 095301 (2012).
 - [3] L. W. Cheuk, A. T. Sommer, Z. Hadzibabic, T. Yefsah, W. S. Bakr, and M. W. Zwierlein, Phys. Rev. Lett. **109**, 095302 (2012).
 - [4] For a review, see J. Dalibard, F. Gerbier, G. Juzeliūnas, and P. Öhberg, Rev. Mod. Phys. **83**, 1523 (2011).
 - [5] B. M. Anderson, I. B. Spielman, and G. Juzeliūnas, Phys.

- Rev. Lett. **111**, 125301 (2013).
- [6] Z.-F. Xu, L. You, and M. Ueda, Phys. Rev. A **87**, 063634 (2013).
- [7] B. M. Anderson, G. Juzeliunas, V. M. Galitski, and I. B. Spielman, Phys. Rev. Lett. **108**, 235301 (2012).
- [8] M. Gong, S. Tewari, and C. Zhang, Phys. Rev. Lett. **107**, 195303 (2011).
- [9] H. Hu, L. Jiang, X.-J. Liu, and H. Pu, Phys. Rev. Lett. **107**, 195304 (2011).
- [10] Z. Q. Yu and H. Zhai, Phys. Rev. Lett. **107**, 195305 (2011).
- [11] C. Qu, Z. Zheng, M. Gong, Y. Xu, L. Mao, X. Zou, G. Guo, and C. Zhang, Nat. Commun. **4**, 2710 (2013).
- [12] W. Zhang and W. Yi, Nat. Commun. **4**, 2711 (2013).
- [13] J. P. Vyasanakere and V. B. Shenoy, Phys. Rev. B **83**, 094515 (2011).
- [14] J. P. Vyasanakere, S. Zhang and V. B. Shenoy, Phys. Rev. B **84**, 014512 (2011).
- [15] Y. Li and C. Wu, Phys. Rev. B **85**, 205126 (2012).
- [16] S. S. Zhang, X. L. Yu, J. Ye, and W. M. Liu, Phys. Rev. A **87**, 063623 (2013).
- [17] X. Cui and T.-L. Ho, Phys. Rev. A **89**, 013629 (2014).
- [18] E. Stoner, Philos. Mag. **15**, 1018 (1993).
- [19] Y. Nagaoka, Phys. Rev. **147**, 392 (1966).
- [20] A. Mielke, J. Phys. A: Math. Gen. **24**, L73 (1991); **24**, 3311 (1991); Phys. Lett. A **174**, 443 (1993).
- [21] H. Tasaki, Phys. Rev. Lett. **69**, 1608 (1992); Phys. Rev. B **40**, 9192 (1989); Commun. Math. Phys. **242**, 445 (2003); A. Tanaka and H. Tasaki, Phys. Rev. Lett. **98**, 116402, (2007).
- [22] H. Katsura and A. Tanaka, Phys. Rev. A **87**, 013617 (2013).
- [23] Y. Li, E. H. Lieb, and C. Wu, arxiv: 1310.4391.
- [24] L. Liu, H. Yao, E. Berg, S. R. White, and S. A. Kivelson, Phys. Rev. Lett. **108**, 126406 (2012).
- [25] G. B. Jo, Y. R. Lee, J. H. Choi, C. A. Christensen, T. H. Kim, J. H. Thywissen, D. E. Pritchard, and W. Ketterle, Science **325**, 1521 (2009).
- [26] R. A. Duine and A. H. MacDonald, Phys. Rev. Lett. **95**, 230403 (2005).
- [27] G. J. Conduit and B. D. Simons, Phys. Rev. Lett. **103**, 200403 (2009).
- [28] S. Pilati, G. Bertaina, S. Giorgini, and M. Troyer, Phys. Rev. Lett. **105**, 030405 (2010).
- [29] D. Pekker, M. Babadi, R. Sensarma, N. Zinner, L. Pollet, M. W. Zwierlein, and E. Demler, Phys. Rev. Lett. **106**, 050402 (2011).
- [30] C. Sanner, E. J. Su, W. Huang, A. Keshet, J. Gillen, and W. Ketterle, Phys. Rev. Lett. **108**, 240404 (2012).
- [31] X. Cui and T.-L. Ho, Phys. Rev. Lett. **110**, 165302 (2013); Phys. Rev. A **89**, 023611 (2014).
- [32] P. Massignan, Z. Yu, and G. M. Bruun, Phys. Rev. Lett. **110**, 230401 (2013).
- [33] J. A. Hertz, Phys. Rev. B **14**, 1165 (1976).
- [34] A. J. Millis, Phys. Rev. B **48**, 7183 (1993).
- [35] U. Zülicke and A. J. Millis, Phys. Rev. B **51**, 8996 (1995).
- [36] It is interesting to compare with the counterpart modes in the conventional Fermi gas without SOC. In the paramagnet side, there is a gapless sound mode, but no collective modes in the spin channel. In the itinerant FM, the sound mode disappears, the symmetry breaking $SU(2)_{spin} \rightarrow U^z(1)_{spin}$ leads to two transverse Goldstone modes with the dispersion $\omega \sim Dq^2$. They are out of the interband PH continuum, so are stable, while the mixed longitudinal-density modes are inside the intra-band PH continuum, so are over-damped.
- [37] F.-D. Sun, X.-L. Yu, J. Ye, H. Fan, W. M. Liu, Scientific Reports **3**, 2119 (2013).
- [38] L. Jiang, L. O. Baksmaty, H. Hu, Y. Chen, and H. Pu, Phys. Rev. A **83**, 061604 (R) (2011).
- [39] J. T. Stewart, J. P. Gaebler, and D. S. Jin, Nature (London) **454**, 744 (2008).
- [40] J. Kinast, A. Turlapov, J. E. Thomas, Q. Chen, J. Stajic, and K. Levin, Science **25**, 1296 (2005).
- [41] M. J. H. Ku, A. T. Sommer, L. W. Cheuk, and M. W. Zwierlein, Science **335**, 563 (2012).
- [42] C.-L. Hung, X. Zhang, N. Gemelke, and C. Chin, Nature (London) **470**, 236 (2011).
- [43] N. Gemelke, X. Zhang, C.-L. Huang, and C. Chin, Nature (London) **460**, 995 (2009).
- [44] C. Sanner, E. J. Su, A. Keshet, W. Huang, J. Gillen, R. Gommers, and W. Ketterle, Phys. Rev. Lett. **106**, 010402 (2011).
- [45] C. Sanner, E. J. Su, W. Huang, A. Keshet, J. Gillen, and W. Ketterle, Phys. Rev. Lett. **108**, 240404 (2012).
- [46] Y. Shin, C. H. Schunck, A. Schirotzek, and W. Ketterle, Nature (London) **451**, 689 (2008).
- [47] A. V. Chubukov, S. Sachdev and J. Ye, Phys. Rev. B **49**, 11919 (1994).
- [48] J. Ye and S. Sachdev, Phys. Rev. Lett. **80**, 5409 (1998).
- [49] J. Ye, Phys. Rev. B **58**, 9450 (1998).
- [50] J. Ye, Phys. Rev. B **60**, 8290 (1999).
- [51] To one-loop level, we obtain the renormalized parameters as: $T(b) = Tb^3$, $\gamma_L(b) = \gamma_L b^{-2}$, $u(b) = ub^{-2}$ and $\delta(b) = b^2[\delta + 2u \int_0^{\ln b} dx e^{-(1+z_T)x} f_T^{(2)}(Te^{z_T x}) + u \int_0^{\ln b} dx e^{-(1+z_L)x} f_L^{(2)}(Te^{z_L x})]$, where, similar to traditional Fermi gas[34], $f_T^{(2)}(t) \simeq f_T^{(2)}(0) + \mathcal{A}_T t^2$ when $t \ll 1$, and $\simeq \mathcal{B}_T t$ when $t > 1$. $f_L^{(2)}(t)$ behaves similarly except its temperature dependence is exponentially small for $t \ll 1$.
- [52] The universal function is defined as: $\Phi(x) = \frac{K_3}{2} \int_0^\infty dt t^{-5/2} \ln[1 - \exp(-\frac{1}{t}\sqrt{1+xt})]$, where $K_3 = 1/2\pi^2$ is an angle integration factor in 3D. The asymptotic form of $\Phi(x)$ in quantum regime I and II, $x \gg 1$, is given by $\Phi(x) \simeq -K_3 C_1 / (2x^{3/2})$, where $C_1 \simeq 4.3292$; while in classical regime III and IV, $x \ll 1$, there is $\Phi(x) \simeq -K_3 C_2 / 2$, where $C_2 \simeq 1.18886$. The irrelevant interaction u provides small corrections near the critical point.
- [53] M. Trinker, S. Groth, S. Haslinger, S. Manz, T. Betz, S. Schneider, I. Bar-Joseph, T. Schumm, and J. Schmiedmayer, Appl. Phys. Lett. **92**, 254102 (2008).